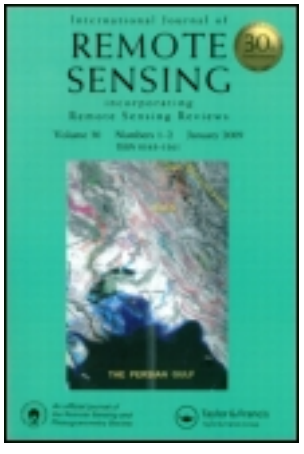

International Journal of Remote Sensing

Publication details, including instructions for authors and subscription information:
http://www.tandfonline.com/loi/tres20

Estimating tropical forest biomass more accurately by integrating ALOS PALSAR and Landsat-7 ETM+ data

Tyas Mutiara Basuki[ab], Andrew K. Skidmore[b], Yousif A. Hussin[b] & Iris Van Duren[b]

[a] Forestry Research Institute of Solo, Jl. A. Yani, Pabelan, Solo, Indonesia

[b] ITC - Geo-Information Science and Earth Observation, University of Twente, 7500 AA, Enschede, The Netherlands

Published online: 05 Apr 2013.

To cite this article: Tyas Mutiara Basuki, Andrew K. Skidmore, Yousif A. Hussin & Iris Van Duren (2013) Estimating tropical forest biomass more accurately by integrating ALOS PALSAR and Landsat-7 ETM+ data, International Journal of Remote Sensing, 34:13, 4871-4888, DOI: 10.1080/01431161.2013.777486

To link to this article: http://dx.doi.org/10.1080/01431161.2013.777486

International Journal of Remote Sensing, 2013
Vol. 34, No. 13, 4871–4888, http://dx.doi.org/10.1080/01431161.2013.777486

Taylor & Francis
Taylor & Francis Group

Estimating tropical forest biomass more accurately by integrating ALOS PALSAR and Landsat-7 ETM+ data

Tyas Mutiara Basuki[a,b]*, Andrew K. Skidmore[b], Yousif A. Hussin[b], and Iris Van Duren[b]

[a]*Forestry Research Institute of Solo, Jl. A. Yani, Pabelan, Solo, Indonesia;* [b]*ITC – Geo-Information Science and Earth Observation, University of Twente, 7500 AA, Enschede, The Netherlands*

(*Received 7 July 2011; accepted 21 December 2012*)

Integration of multisensor data provides the opportunity to explore benefits emanating from different data sources. A fusion between fraction images derived from spectral mixture analysis of Landsat-7 ETM+ and phased array L-band synthetic aperture radar (PALSAR) is introduced. The aim of this fusion is to improve the estimation accuracy of above-ground biomass (AGB) in lowland mixed dipterocarp forest. Spectral mixture analysis was applied to decompose a mixture of spectral components of Landsat-7 ETM+ into vegetation, soil, and shade fractions. These fraction images were integrated with PALSAR data using the discrete wavelet transform (DWT) and Brovey transform. As a comparison, spectral reflectance of Landsat-7 ETM+ was fused directly with PALSAR data. Backscatter of horizontal–horizontal and horizontal–vertical polarizations was also used to estimate AGB. Forest inventory was carried out in 77 randomly distributed plots, the data being used for either model development or validation. A local allometric equation was applied to calculate AGB per plot. Regression models were developed by integrating field measurements of 50 sample plots with remotely sensed data, e.g. fraction images, reflectance of Landsat-7 ETM+, and PALSAR data. The models developed were validated using 27 independent sample plots. The results showed that not all fused images significantly improved the accuracy of AGB estimation. The model based on Brovey transform using the reflectance of Landsat-7ETM+ and PALSAR produced an R^2 of only 0.03–0.10. By contrast, fusion between PALSAR data and fraction images using Brovey transform improved the accuracy of R^2 to 0.33–0.46. Further improvement in the accuracy of estimating AGB was observed when DWT was applied to integrate PALSAR with the reflectance of Landsat-7ETM+ ($R^2 =$ 0.69–0.72) and PALSAR with fraction images ($R^2 = 0.70$–0.75).

1. Introduction

Biomass estimation in tropical forests has become a topic of great interest because its carbon stock forms part of the global carbon cycle. Forests can exchange carbon with the atmosphere through forest degradation and deforestation (Luckman et al. 1998; Phat, Knorr, and Kim 2004) and forest regrowth (Luckman et al. 1998; Schimel et al. 2001). The use of optical and microwave remote sensing in combination with field measurements may provide a method to improve estimation of forest biomass over large areas (Rauste 2005). However, in biomass assessment, data derived from these sensors have both advantages and disadvantages.

*Corresponding author. Email: basuki@itc.nl; tmbasuki@yahoo.com

Optical sensors with medium spatial resolution, such as Landsat-7 ETM+, have multispectral bands in the visible, near infrared, middle infrared, and thermal infrared. Synthetic aperture radar (SAR) penetrates through surficial materials and vegetation canopies and can provide information on surface roughness, volume, and mass of objects, as well as moisture content. Optical sensors collect reflected solar energy which cannot penetrate into vegetation canopies, cloud, haze, and fog. Another disadvantage of optical medium spatial resolution imagery is that reflectance recorded by a sensor within a single pixel may be a combination of the reflectance by pure components on the ground surface in that pixel. Decomposition of pixels into their separate components followed by quantification of the vegetation fraction is a crucial step before employing these data for biomass estimation (Lu, Batistella, and Moran 2005). In tropical forests, the complex forest structure causes canopy shading, influencing vegetation reflectance captured by a sensor. This could have an affect on biomass estimation (Gemmell 1995; Steininger 2000).

The application of SAR to assess biomass offers opportunities for biomass estimation in tropical regions where high cloud cover often occurs. Radar is an active microwave system that can work during both day and night, independent of solar energy. It can penetrate clouds and record energy returned from surface features. Besides these advantages, SAR also has limitations, such as in hilly regions, where no information is recorded at all in radar shadow areas (Trevett 1986).

SAR has been employed to assess biomass in different regions. For instance, it has been applied in Australia to estimate biomass of eucalyptus forests (Austin, Mackey, and van Nief 2003) and woody vegetation in the Southern Brigalow Belt, Central Queensland (Liang et al. 2005; Lucas et al. 2006), in Canada's western sub-arctic and low arctic region (Chen et al. 2009), in pine forests in the USA (Hyde et al. 2007), and in the Huvsgul Lake Basin, Mongolia, on taiga species (Tsolmon, Tateishi, and Tetuko 2002). In tropical Amazon forests in Brazil, Kuplich, Curran, and Atkinson (2005) and Santos et al. (2003) have employed SAR for estimating forest biomass. Regarding its application in these tropical forests, the above-ground biomass (AGB) can be estimated with reasonable accuracy using cross-polarized L- and P-band SAR imagery. However, saturation in biomass estimation is an important issue when computation is directly derived from simple regression between AGB and coefficient backscatter. The shorter the wavelength, the faster the point of saturation is reached (Kellndorfer et al. 2003; Lu 2006; Lucas et al. 2006). Luckman et al. (1998) observed that backscatter of JERS-1 SAR through horizontal–horizontal (HH) polarization saturated at an AGB of around 60 t ha^{-1} in tropical forest. The point of saturation in biomass estimation is affected by wavelength (e.g. C, L, and P bands), polarization (e.g. HH, horizontal–vertical (HV), and vertical–vertical), incidence angle, and the characteristics of vegetation structure and ground conditions (Lu 2006; Lucas, Moghaddam, and Cronin 2004; Rosenqvist et al. 2003; Saatchi et al. 2011). Fusion between remotely sensed data derived from optical and radar sensors may reduce the problems mentioned above and improve the accuracy of biomass estimation in tropical forests (Lu, Batistella, and Moran 2005; Rauste 2005).

Fusion uses an algorithm to integrate two or more different images to form a new image (Pohl and Genderen 1998). The aim of fusion is to integrate spatial and spectral information (Acerbi-Junior, Clevers, and Schepmna 2006) and to provide complementary information about a surface (Chibani 2006; Pajares and de la Cruz 2004). Fusion is also used to obtain better visual analysis and more accurate classification of land cover (Pradhan et al. 2006). Chavez, Sides, and Anderson (1991) highlighted some points to consider when integrating information from different sensors: digital images from both sensors should be geometrically corrected to match one another, the method applied to fuse the images should

not distort the spectral characteristics of the multispectral image, and the resulting image should have a high spatial resolution and similar spectral properties to the original image.

Various methods have been employed to fuse images. Standard methods include intensity hue saturation, principle component analysis, and Brovey transforms (Hussin and Shaker 1996; Li, Kwok, and Wang 2002; Musa, Hussin, and Weir 2004; Wang et al. 2005). The standard fusion methods mentioned above tend to distort colour information (Amolins, Zhang, and Dare 2007), and sometimes the resulting image cannot preserve the spectral characteristics of the original multispectral data (Kumar, Kartikeyan, and Majumdar 2000). A relatively new approach to fusing images is wavelet transform (Alparone et al. 2004; Amolins, Zhang, and Dare 2007; Li, Kwok, and Wang 2002; Pradhan et al. 2006; Yunhao et al. 2006). Ranchin and Wald (2000) demonstrated that fusion based on wavelet transform could improve spatial resolution with minimum distortion of spectral characteristics of the original image. The basic concept of wavelet decomposition is to analyse the signal according to different scales or resolutions (Martínez and Gilabert 2009). Wavelet fusion decomposes high spatial and multispectral resolution into the same spatial resolution by means of wavelet transform. Detailed information on high spatial resolution data is injected into a multispectral image (Amolins, Zhang, and Dare 2007). To integrate the data, corresponding wavelet coefficients are combined, and the fused image is obtained by performing inverse wavelet transform (Canty 2010; Li, Kwok, and Wang 2002; Ranchin and Wald 2000).

Fusion using wavelet transform has usually been applied to optical remotely sensed data (Lemeshewsky 1999; Ranchin and Wald 2000). It integrates panchromatic images of high spatial resolution with multispectral resolution images of low spatial resolution (Li, Kwok, and Wang 2002; Núñez et al. 1999; Shi et al. 2003). Recently, SAR has been fused with images derived from optical sensors using wavelet transform (Alparone et al. 2004; Chibani 2005, 2006; Simone et al. 2002). Fusion with this transform is commonly employed to enhance features in urban areas and for land-cover classification. Chibani (2005) enhanced the detection of lines, edges, and field boundaries on RADARSAT images by fusing this radar with panchromatic images of SPOT based on wavelet transform. Classification accuracy increased when Cakir et al. (1999) conducted wavelet transform to integrate SPOT XS with SAR imagery, and Huang, Zhang, and Li (2008) fused Quick Bird with IKONOS. Based on the reviewed literature, the potential use of image fusion has not been explored sufficiently for quantitative purposes, such as quantifying of forest biomass.

Based on the weaknesses of data derived from optical and microwave sensors as mentioned above, as well as the lack of potential use of image fusion, an innovative approach to quantification of AGB is proposed. The objective of the research is to improve the accuracy in estimating AGB in dipterocarp forests by integrating phased array L-band synthetic aperture radar (PALSAR) with Landsat-7 ETM+. The reason for fusing these data is that PALSAR has longer wavelengths, can penetrate deeper into canopies, and has a higher spatial resolution than Landsat-7 ETM+ data. On the other hand, since optical data have multispectral bands, combining these data types has the potential to achieve higher accuracy in biomass estimation. An innovative approach in this research was that the spectral reflectance of Landsat-7 ETM+ was not directly fused with PALSAR data. Before fusing, the mixture of spectral components present in the pixels of the Landsat-7 ETM+ image was decomposed into vegetation, soil, and shade fractions using spectral mixture analysis. Then, the fraction images resulting from the decomposition were integrated with PALSAR data using Brovey and discrete wavelet transforms. For comparison, the spectral reflectance of Landsat-7 ETM+ was directly fused with PALSAR data, and AGB was estimated using backscatter from HH and HV polarizations only.

2. Methods

2.1. Study area

The study area is located in the Labanan forest concession managed by PT Hutan Sanggam Labanan Lestari, Berau Regency, East Kalimantan, Indonesia. However, the area was extended (Figure 1) beyond this forest concession to fulfil the prerequisites for the application of discrete wavelet transform (DWT) to the fusion. Most of the forests were logged using a selective cutting and replanting system between 1976 and 2003, while the rest remained unlogged.

The forest type of the study area is lowland mixed dipterocarp forests. Dipterocarpaceae and Euphorbiaceae are the first and second most abundant families in these forests (Sist and Saridan 1998). Species richness in the study area is high, with 182 tree species (DBH ≥ 10 cm) per hectare in undisturbed forests (Bertault and Kadir 1998). These forests consist of commercial, non-commercial, and protected species.

2.2. Image pre-processing

Landsat-7 ETM+ and PALSAR images were used in this research. A Landsat-7 ETM+ image acquired on 31 May 2003, from path 117 and row 59, was used to complement the PALSAR images. The PALSAR images were acquired on 12 June 2007. The forest was assumed to be in a stable condition, as forest harvesting had not been allowed in this concession between 2004 and the acquisition of PALSAR data.

Image processing was conducted to minimize geometric and radiometric errors. Geometric correction of the Landsat-7 ETM+ image was conducted using 15 ground control points (GCPs) resulting in a pixel error below 0.5. The first-order polynomial of a geometric model was applied and the image was geocoded to the Universal Transverse Mercator (UTM) coordinate system with datum WGS 1984 and zone 50 north. The digital numbers (DNs) of the image were converted to radiance and then to reflectance using an exo-atmospheric model as described in NASA (2005). DN values of bands 1, 2, 3, 4, 5, and 7 of Landsat-7 ETM+ were converted into reflectance.

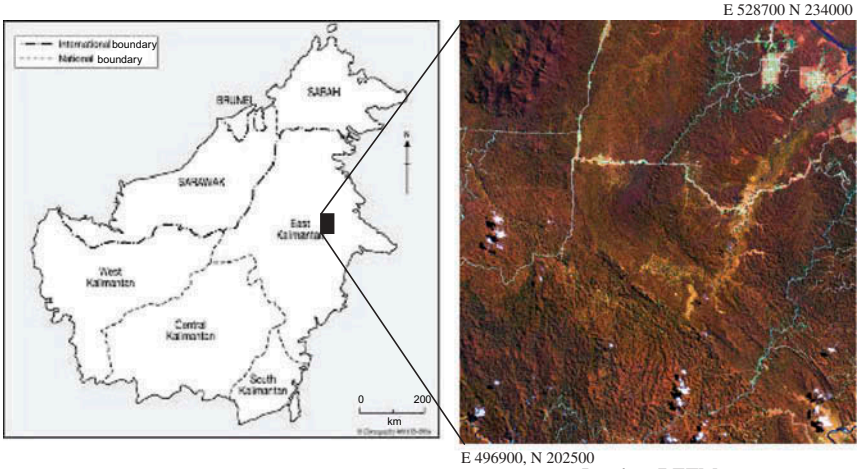

Figure 1. Location of the study area.

The PALSAR image was received in level 1.1, which is in a slant range projection. Its spatial slant and azimuth resolutions were 9.50 m and 4.50 m, respectively. This L-band image had an incidence angle of 38.76°, with like polarization (HH) and cross-polarization (HV). Conversion from slant range to ground projection was conducted using the Alaska Satellite Facility (ASF) MapReady version 2.2.5. This free software (http://www.asf.alaska.edu/sardatacenter/softwaretools, accessed 8 November 2009) was also employed to correct terrain and radiometric distortions, as well as for geocoding. This image was radiometrically calibrated by converting amplitude values DNs into a power image in units of σ_0, which is the ratio between the power transmitted back from a patch of ground and that transmitted to it (Alaska Satellite Engineering Group, http://www.asf.alaska.edu/sardatacenter/softwaretools, accessed 8 November 2009). The conversion of DNs to σ_0 (in power scale) is given as

$$\sigma_0 = a_2(\mathrm{DN}_2 - a_1 N_\mathrm{r}), \tag{1}$$

where DN is the original pixel value, N_r is the noise as a function of range, a_1 is the noise scale factor, and a_2 is the linear conversion determined during calibration of the processor. The σ_0 amplitude values act as independent variables in the prediction of AGB (Fransson, Walter, and Ulander 2000).

SAR is acquired in a lateral direction and induces distortions of rough terrain in the image such as foreshortening, shadow, and layover. In this case, terrain correction was carried out to minimize these distortions. The image was corrected using heights obtained from a digital elevation model (DEM). The DEM had a 30 m spatial resolution and was derived from ASTER data freely downloaded from http://www.gdem.aster.ersdac.or.jp (accessed 10 November 2009). Radiometry of the PALSAR was corrected using local incidence angles derived from the DEM. Kellndorfer, Pierce, and Dobson (1998) formulated this as follows:

$$\sigma_\mathrm{corr} = \sigma_\mathrm{orig} \sin(\alpha_\mathrm{DEM}) / \sin(\alpha_\mathrm{ELL}), \tag{2}$$

where σ_corr is the radar backscatter coefficient corrected for local incidence angle, σ_orig is the original backscatter coefficient, α_ELL is the incidence angle measured from the ellipsoid, and α_DEM is the actual incidence angle calculated from the DEM.

The image was geocoded into the UTM coordinate system with datum WGS 1984 and zone 50 N. It was resampled using the nearest neighbour method to produce an image with a spatial resolution of 16 m. This was a requirement for the wavelet analysis, as explained in the next section. In order to fuse the images, PALSAR was registered to LANDSAT-7 ETM+ by a second-order polynomial. The errors in the x and y directions were 4.71 and 4.60 m, respectively, with a total root mean squared error (RMSE) of 6.58 m.

2.3. *Spectral mixture analysis*

For remotely sensed data with medium resolution such as Landsat-7 ETM+, a signal from within a pixel recorded by the sensor could be a combination of the reflectance from all component endmembers on the earth's surface covered by that pixel. An endmember is a pure spectral component (Adams and Gillespie 2006). Spectral mixture analysis decomposes mixture endmembers. In spectral mixture analysis, it is assumed that a pixel in each spectral band is linear combinations of multiple components weighted by relative surface abundance and is expressed as (Tompskins et al. 1997)

$$R_b = \sum_{i=1}^{m} f_i r_{ib} + E_b, \tag{3}$$

where R_b is the reflectance of a pixel at band b, f_i is the fractional abundance of endmember i (from a total of m endmembers), r_{ib} is the reflectance at band b of endmember i, and E_b is the error in band b of the model fit.

Reflectance bands 1, 2, 3, 4, 5, and 7 of Landsat 7 ETM+ were transformed using minimum noise fraction. The transformed image was used to determine the most spectrally pure pixel, using the pixel purity index (Boardman, Kruse, and Green 1995). Pixels having high purity index values were used to identify the location of sample endmembers on the original image (Souza, Roberts, and Cocrane 2005). In addition, sample endmembers were also identified by their location on the extremes of the image feature space (Lu, Batistella, and Moran 2005). The sample endmembers selected were used to decompose the mixed spectral reflectance of the original image and produce fraction images consisting of vegetation, soil, shade, and error fractions. All of the procedures for the spectral mixture analysis mentioned above were run using Environment for Visualizing Images (ENVI) 4.7 and Interactive Data Language (IDL) 7.1 software (EXELIS 2013). Only forest areas were used for further analysis, whereas water bodies, settlements, shrubs, and roads were masked out.

2.4. The Brovey transform

The Brovey transform is intended to produce red, green, and blue images; therefore only three bands at a time should be merged from the input multispectral data (Leica Geosystem 2008). To choose three bands for the Brovey transform, a correlation analysis between each band of Landsat-7 ETM+ with AGB was carried out. The three bands of Landsat-7 ETM+ with the highest correlation to AGB were employed to fuse with the HH and HV polarizations of the PALSAR images. In addition, the fraction images (vegetation, soil, and shade) resulting from spectral mixture analysis were also used as input in this fusion. The formulas (modified from Leica Geosystem 2008) are

$$[\mathrm{B1}/\mathrm{B1} + \mathrm{B2} + \mathrm{B3}] \times [\text{High resolution image}] = \mathrm{B1\_new}, \tag{4}$$

$$[\mathrm{B2}/\mathrm{B1} + \mathrm{B2} + \mathrm{B3}] \times [\text{High resolution image}] = \mathrm{B2\_new}, \text{and} \tag{5}$$

$$[\mathrm{B3}/\mathrm{B1} + \mathrm{B2} + \mathrm{B3}] \times [\text{High resolution image}] = \mathrm{B3\_new}, \tag{6}$$

where B1, B2, and B3 are bands of the Landsat-7 ETM+ or fraction images, the high-resolution image is HH and HV polarization of PALSAR, and B1_new, B2_new, and B3_new are the bands resulting from Brovey transform. The algorithm of the Brovey transform is simple, and it can improve visual interpretation of images, although it may distort reflectance when applied to image fusion.

2.5. DWT and its application to image fusion

A wavelet is a local wavelike function and its transform is a convolution of the wavelet function with a signal (Addison 2002). During decomposition, the wavelet may be moved

along the signal (translated) and be stretched or squeezed (dilated) (Addison 2002; Mallat 1989). Basically, wavelet transform quantifies the matching of the wavelet with the signal at different locations and scales (Addison 2002; Pittiglio et al. 2012). A strongly positive wavelet coefficient will be produced if the wavelet matches the shape of the signal, while in contrast a strongly negative coefficient will be obtained if the wavelet and signal are out of phase (Addison 2002; Pittiglio et al. 2012). In addition, the transform yields a low coefficient if the wavelet and signal do not coincide.

DWT transforms signals over a discrete set of scales, and the transforms can be realized using a variety of fast algorithms and customized hardware (Bruce, Morgan, and Larsen 2001; Pu and Gong 2004). An application of DWT for image fusion can be illustrated as a bank of filters, where at every level of decomposition the signal is split into high- and low-frequency components. Further decomposition can be applied to the low-frequency components until the desired resolution is reached, as explained in detail by Mallat (1989), Strang and Nguyen (1997), Shensa (1992), and Amolins, Zhang, and Dare (2007). The original image can be reconstructed by inverse transformation of all of the components of each deconstructed level in turn, starting from the coarsest spatial resolution (Amolins, Zhang, and Dare 2007).

A prerequisite for the DWT is that the transform convolves the data by a factor of 2^n for the integer of n (Addison 2002; Canty 2010). Four quadrants are generated from every spatial resolution level of decomposition (Chibani and Houacine 2003; Canty 2010). These quadrants consist of one approximate image (low resolution and a reproduction of the original), and three detailed images (horizontal, vertical, and diagonal detail) (Chibani and Houacine 2003; Pittiglio et al. 2012).

In image fusion, detailed information from one image (with high spatial resolution) can be extracted and injected into low spatial resolution or multispectral resolution images (Chibani 2005; Amolins, Zhang, and Dare 2007). The details of an image generally characterize different physical structures of the scene (Mallat 1989); therefore, the resulting fused image contains information complementary to the fine and coarse resolution images. In this study, the PALSAR image is a high spatial resolution image and the Landsat-7 ETM+ image, as well as the fraction images resulting from spectral mixture analysis, are multispectral images with low spatial resolution. The orthogonal wavelet transform was applied to the PALSAR image, the original reflectance of the Landsat-7 ETM+ data, and to the image resulting from spectral mixture analysis. PALSAR was downscaled twice and the data from the optical remotely sensed data were decomposed once to achieve 64 m spatial resolution. Images from PALSAR were fused with the optical remotely sensed imagery. Finally, an inverse transform was applied to reconstruct a fused image with high spatial resolution. A weighted model was employed in the inverse transform (Amolins, Zhang, and Dare 2007; Canty 2010) using the equation

$$C^Z_{\text{optical}} = a^Z \times C^Z_{\text{PALSAR}} + b^Z, \text{ for } Z = \text{D, V, and H,} \tag{7}$$

where $C^Z{}_{\text{optical}}$ is the optical remotely sensed imagery with information injected, $C^Z{}_{\text{PALSAR}}$ is the detailed image of PALSAR, a^Z is the mean of the optical remotely sensed data, b^Z is the standard deviation of the PALSAR data, and D, V, and H are the diagonal, vertical, and horizontal directions, respectively.

The wavelet transform can be applied to describe and characterize spatial pattern in an ecological system, such as forest canopy structure (Bradshaw and Spies 1992). Another advantage of this method is that the magnitude of the signal can be directly related to its

position in the image (Pittiglio et al. 2012). Besides the advantages, however, the wavelet transform has one disadvantage: it cannot detect a dominant pattern smaller than the original pixel size (Strand et al. 2006).

2.6. Forest inventory

Field work was conducted from May to June 2006. Random sample plot allocation was based on a Landsat-7 ETM+ image (31 May 2003). The image acquired in 2003 was used because, for the present study area, no cloud-free image had been acquired between that date and the field campaign. Seventy-seven sample plots were divided randomly into two groups: 50 were used as training samples and 27 for validation. The coordinates of the plots were recorded using the global positioning system (GPS).

The size of each plot was 500 m^2 and circular, but with corrections for slope of the terrain. The radius ranged from 12.62 to 15.78 m. Within each of the 77 plots, tree diameter equal to or greater than 10 cm was measured at breast height (DBH). Based on the forest inventory, the DBH of the sample plots ranged from 10 to 192 cm. The DBH data from the forest inventory were converted to AGB using a local allometric equation (Basuki et al. 2009). The equation for estimation of total above ground biomass (TAGB) is

$$\ln(\mathrm{AGB}) = 2.196 \times \ln(\mathrm{DBH}) - 1.201, \tag{8}$$

where AGB is the dry weight of AGB (kg $tree^{-1}$) and DBH is in centimetres. The level of AGB was obtained by de-transforming ln (AGB) values (Basuki et al. 2009). The estimated AGB was used as the reference data, and descriptive statistics are provided in Table 1. Paired *t*-testing at 95% confidence interval indicated that there were no differences between the training and the validation data.

2.7. Analysis

Regression models were developed to examine the relationships between dependent variables (AGB) and independent variables. Independent variables were the amplitude backscatter values of HH and HV polarizations from the PALSAR data, and the single- and multiple-band combinations of the fused images using the Brovey and wavelet methods. Multiple regressions were proposed after examining free multicollinearity among the independent variables. Independent variables were the average of the extracted values from 3 × 3 pixels around the centre points of the sampling plots (Tsolmon, Tateishi, and Tetuko 2002; Austin, Mackey, and van Nief 2003; Lucas et al. 2006). Every model was cross-validated using an independent data set ($n = 27$).

Table 1. Descriptive statistics of above-ground biomass (t ha^{-1}) for training (50 plots) and validation (27 plots) data.

Above-ground biomass	Training samples	Validation samples
Minimum	102.62	102.26
Mean	343.79	329.20
Maximum	839.32	812.15
Standard deviation	156.61	191.98

Table 2. Pearson correlation at 95% of confidence interval between above-ground biomass (t ha^{-1}) and individual spectral reflectance of Landsat-7 ETM+ for 50 sample plots.

Band	Pearson correlation	*p*-value
1	0.205	0.076
2	0.231	0.053
3	−0.097	0.252
4	0.757	0.000
5	0.564	0.000
7	0.369	0.040

3. Results

3.1. *Fused images*

The highest correlation between the spectral reflectance of Landsat-7 ETM+ and AGB was observed in band 4, followed by bands 5 and 7 as shown in Table 2. Therefore, the reflectance of these bands and the PALSAR data were used as input for the Brovey transform. This transformation was also applied to integrate the fractions of vegetation, soil, and shade with the HH and HV polarizations.

In agreement with previous studies (Kumar, Kartikeyan, and Majumdar 2000; Ranchin and Wald 2000; Li, Kwok, and Wang 2002), fusion using the Brovey transform distorted the characteristics of radiometry of the multispectral image, as illustrated in Figure 2(*c*). However, fusion using this transform yielded a better visual performance of the resulting image when the PALSAR data were integrated with the fraction image from the spectral mixture analysis (compare Figures 2(*b*) and (d)). Fusion, using DWT, produced a similar result visually to the multispectral image. In this case, Figure 2(*a*) should be compared with 2(e), and 2(b) with 2(f).

3.2. *Biomass retrieval using remote sensing signal*

The proposed models integrating fractional images with PALSAR data (Table 3) have greatly improved the estimation of AGB compared with the single polarization of PALSAR, for both Brovey and discrete wavelet transforms. R^2 was increased when PALSAR data were incorporated in the fractional images, rather than using the original spectral reflectance of Landsat-7 ETM+. However, the model derived from the Brovey transform had a lower coefficient of determination than that of single- and multiple-band combination estimators resulting from DWT. By contrast, only weak correlation was observed between AGB and radar backscatter of both HH polarization ($R = 0.268$) and HV polarization ($R = 0.363$); therefore the proposed models were derived only from the fused images, as shown in Table 3.

Fusion using wavelet transform between the original reflectance of Landsat-7 ETM+ and HV polarization produced a higher R^2 than with HH polarization (Table 3). However, fusion using wavelet transform between fraction images with HV polarization did not always provide a higher R^2 than those of HH polarization. For the model based on spectral mixture analysis and wavelet transformation, multiple regressions of the fraction images increased the coefficient of determination. However, the highest R^2 of the proposed models was achieved through multiple regression of the vegetation and soil fractions with the radar backscatter using DWT. Multiple regressions were also conducted on the fused image of fraction images with HH and HV polarization, and this produced an R^2 of 0.752. However,

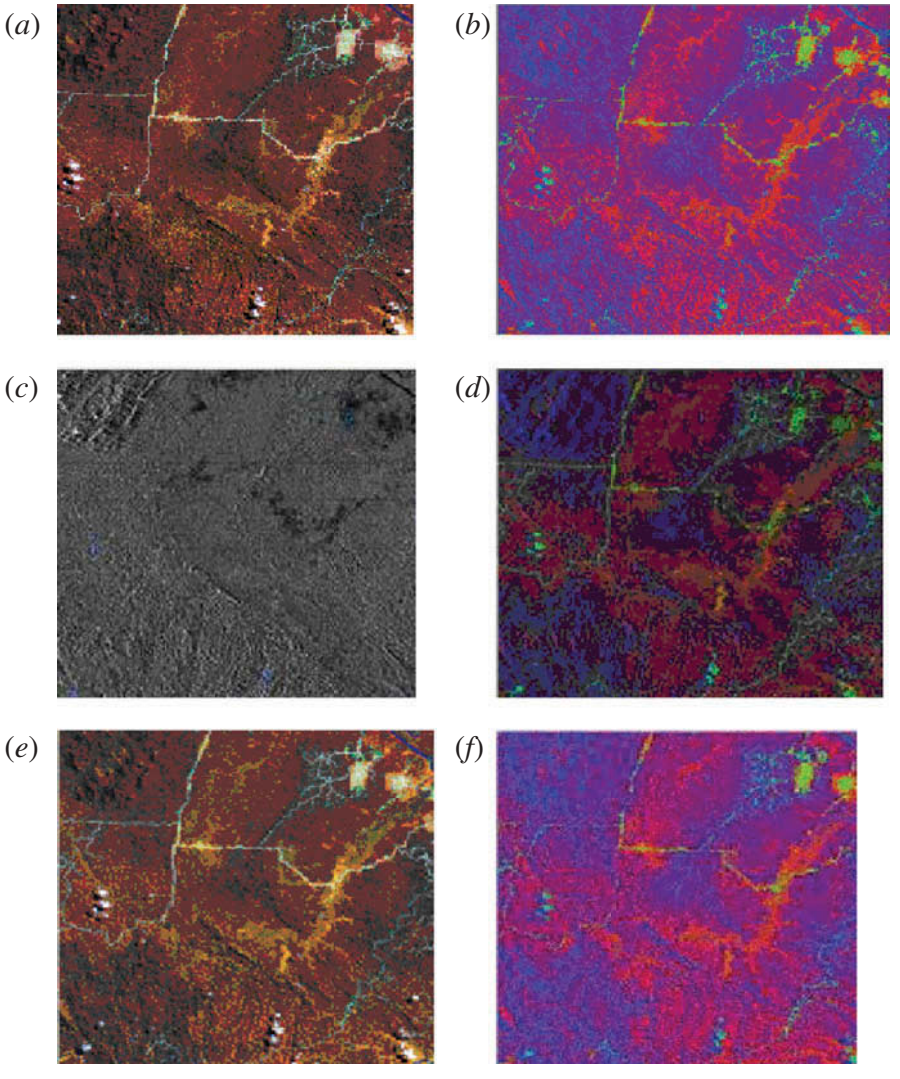

Figure 2. Original Landsat-7 ETM+ image (*a*); fraction image resulting from spectral mixture analysis (*b*); fusion of HV polarization of PALSAR with reflectance of bands 4, 5, and 7 of Landsat-7 ETM+ using the Brovey transform (*c*); fraction image resulting from spectral mixture analysis using Brovey transform (*d*); reflectance of Landsat-7 ETM+ using discrete wavelet transform (*e*); and fraction image resulting from spectral mixture analysis using discrete wavelet transform (*f*).

due to multicollinearity between those fractions, the model was excluded. Table 3 also shows the models based on fraction images derived from spectral mixture analysis. This is to provide a clearer comparison between models based on fusion and those based on non-fusion images.

Validation was tested using 27 sample plots of independent data for the fused images. Although the model based on the fusion of fractional images with HV polarization using the Brovey transform has a fair correlation with AGB ($R^2 = 0.461$), validation using the independent data set yielded a high RMSE (Table 4). Compared with the models based on Brovey transform, those based on fraction images reduced the RMSE of the validation from 28% to 35%.

Table 3. Regression models at 95% of confidence interval between fused images (spectral reflectance of Landsat-7 ETM+ or fraction images and PALSAR data) and above-ground biomass (t ha^{-1}) using 50 sample plots.

Method	Independent variable	Equation	Adjusted R^2	p-value	RMSE (t ha^{-1})	RMSE (% of mean)
Brovey transform	Fusion of reflectance bands 4, 5, and 7 with HH polarization	–	0.031	0.220	154.2	45.2
	Fusion of reflectance bands 4, 5, and 7 with HV polarization	–	0.101	0.049	148.5	43.4
	Fusion of vegetation, soil, and shade fractions with HH polarization	AGB = 167.654 + 2363.802brov_veg_soil_shade_hh	0.332	0.000	128.0	37.8
	Fusion of vegetation, soil, and shade fractions with HV polarization	AGB = 123.910 + 16014.500brov_veg_soil_shade_hv	0.461	0.000	114.9	33.9
Discrete wavelet transform	Fusion of reflectance band 4 with HH polarization	AGB = –1352.896 + 7162.091*ref4_hh	0.691	0.000	87.1	25.5
	Fusion of reflectance bands 4, 5, and 7 with HH polarization	AGB = –1439.984 +7683.668*ref4hh + 1968.451*ref5_hh – 7439.332*ref7_hh	0.699	0.000	85.9	25.2
	Fusion of reflectance bands 1, 2, 3, 4, 5, and 7 with HH polarization	AGB = –252.822–9358.546*ref1_hh – 3910.356*ref2_hh – 8260.823*ref3_hh + 8005.990*ref4_hh – 6553.968*ref5_hh – 5097.623*ref7_hh	0.702	0.000	85.5	25.1
	Fusion of reflectance band 4 with HV polarization	AGB = –1353.881 + 7143.904*ref4_hv	0.720	0.000	82.8	24.3
	Fusion of reflectance bands 4, 5, and 7 with HV polarization	AGB = –132.133 + 8201.965*ref4_hv – 2356.026*ref5_hv – 1816.364*ref7_hv	0.719	0.000	83.0	24.3
	Fusion of reflectance bands 1, 2, 3, 4, 5 and 7 with HV polarization	AGB = –940.170– (6459.237*ref1_hv) +(5211.665*ref2_hv) –(5577.381*ref3_hv) + 8085.999*ref4_hv –1687.023*ref5_hv – 881.406*ref7_hv	0.711	0.000	84.2	24.7
	Fusion of vegetation fraction with HH polarization	AGB = –191.764 + 1152.929*veg_hh	0.704	0.000	85.3	25.0

(*Continued*)

Table 3. (*Continued*).

Method	Independent variable	Equation	Adjusted R^2	*p*-value	RMSE (t ha^{-1})	RMSE (% of mean)
	Fusion of vegetation and soil fractions with HH polarization	AGB = –83.304 + 1073.298*veg_hh – 1436.975*soil_hh	0.746	0.000	78.9	23.1
	Fusion of vegetation, soil and shade fractions with HH polarization	AGB = –198.478 + 1187.383*veg_hh – 1382.406*soil_hh + 125.005*shade_hh	0.742	0.000	79.6	23.3
	Fusion of vegetation fraction with HV polarization	AGB = –180.053 + 1116.703*veg_hv	0.710	0.000	84.3	24.7
	Fusion of vegetation and soil fractions with HV polarization	AGB = –93.942 + 1075.756*veg_hv – 1253.127*soil_hv	0.743	0.000	79.4	23.3
	Fusion of vegetation, soil and shade fractions with HV polarization	AGB = –348.334 + 1313.120*veg_hv – 1175.127*soil_hv + 288.930*shade_hv	0.744	0.000	79.3	23.2
SMA	Vegetation fraction	AGB = –258.055 +1350.342*veg	0.632	0.000	94.9	28.0
	Vegetation and soil fractions	AGB = –200.793 + 1303.543*veg – 723.260*soil	0.635	0.000	94.7	27.9

Notes: AGB, above-ground biomass; brov, Brovey transform; HH, horizontal–horizontal polarization; HV, horizontal–vertical polarization; ref, reflectance; RMSE, root mean squared error; soil, soil fraction; shade, shade fraction; SMA, spectral mixture analysis; veg, vegetation fraction.

Table 4. Validation using an independent data set from 27 plots.

Method	Independent variable	RMSE (t ha^{-1})	RMSE mean (%)
Brovey transform	Fusion of vegetation, soil, and shade fractions with HH polarization	200.92	59.3
	Fusion of vegetation, soil, and shade fractions with HV polarization	188.39	55.6
Discrete wavelet transform	Fusion of reflectance band 4 with HH polarization	123.5	36.5
	Fusion of reflectance bands 4, 5, and 7 with HH polarization	118.3	34.9
	Fusion of reflectance bands 1, 2, 3, 4, 5, and 7 with HH polarization	117.3	34.6
	Fusion of reflectance band 4 with HV polarization	120.0	35.4
	Fusion of reflectance bands 4, 5, and 7 with HV polarization	119.0	35.1
	Fusion of reflectance bands 1, 2, 3, 4, 5, and 7 with HV polarization	117.0	34.5
	Fusion of vegetation fraction with HH polarization	117.0	34.5
	Fusion of vegetation and soil fractions with HH polarization	122.7	36.2
	Fusion of vegetation, soil, and shade fractions with HH polarization	122.9	36.3
	Fusion of vegetation fraction with HV polarization	118.6	35.0
	Fusion of vegetation and soil fractions with HV polarization	121.2	35.8
	Fusion of vegetation, soil, and shade fractions with HV polarization	127.7	37.7
Spectral mixture analysis	Vegetation fraction	130.5	38.5
	Vegetation and soil fractions	135.6	40.1

4. Discussion

Overall, the proposed regression models using the fusion of fraction images improved the estimation accuracy of AGB more than fused images using the original spectral reflectance. This shows that the proportion of mixed spectral components (e.g. vegetation, soil, and shade) should be computed before integration with the PALSAR data in order to achieve higher accuracy of AGB estimation. Separation of the mixed spectral component is essential because most study areas are forests that have previously been logged. In selectively logged forests the ground is not totally covered by trees. Such logged forests are a mix of vegetation, soil, and shade, and on medium-resolution imagery these spectral components are also mixed. For example, Vega (2005) found that felling a single tree in such forests created a gap ranging from 30% to 100% for pixels with a resolution of 15 m. Within this gap, reflectance from the soil may be mixed with that from the surrounding trees and recorded within a pixel by the sensor.

Fusion using DWT improves the estimation accuracy of AGB. This indicates that the data from these two sensors complement each other and that their integration is beneficial.

Landsat-7 ETM+, with its multispectral bands, provides information on different properties of the Earth's surface. For instance, the near-infrared band is useful to detect vegetation with its high reflectance. The information from these multispectral bands is complemented by PALSAR data. The benefit of using the L- band of PALSAR is not only its ability to penetrate deeper into the canopy, but also the nature of SAR data showing multiple scattering within the canopy. Penetration of microwave radiation into the canopy depends on the wavelength and type of polarization (Balzter et al. 2003).

In addition to the above explanation, the wavelet method preserves high- and low-frequency features during spectral decomposition, which means that variation in AGB directly causes change in spectral characteristics, i.e. change in the peaks and valleys along the spectral curve (Pu and Gong 2004). The weaker relationship between total AGB and independent variables extracted from the fused image using the Brovey transform is caused by the algorithm used to enhance the visual interpretation of the combination of red, green, and blue (Wang et al. 2005). Colour distortion can occur if the Brovey transform is employed to fuse multisensor data with large differences in spectral range (Alparone et al. 2004). With respect to the integration data, it can be seen that fusion does not always improve the resulting image as the AGB estimator: this depends on the method applied to integrate data. In the present study, the Brovey transform was unable to properly integrate the advantages of PALSAR and Landsat-7 ETM+ to the fused image. Therefore, models based on fusion between PALSAR and fraction images using the Brovey transform cannot produce higher R^2 compared with the model based only on fraction images.

Using data from single polarization, HV produced higher correlation with AGB than did HH polarization. Most HH polarization responses consist of surface scattering, while HV reflects volumetric multiple scattering. Therefore, cross-polarized data are responding to volume and biomass, especially with the L-band, since they penetrate the forest canopy (Lucas et al. 2006).

Regarding the application of a single L-band from SAR data, Luckman et al. (1998) found that the HH-polarized L-band of JERS-1 SAR saturated at a total AGB of 60 t ha^{-1} in Amazon forests in Brazil. In woodland areas in Queensland, Australia, Lucas et al. (2006) observed that the maximum saturation level for HH and HV polarization of the L-band was 75–80 and 98 t ha^{-1}, respectively. Higher levels of saturation were encountered by Wang and Qi (2008) when applying a modified radiative transfer model using the L-band of JERS-1 SAR in dense moist evergreen forests. By removing leaf contribution from the backscattering coefficient, the saturation level increased. Using this model, the increase in woody backscatter was not reduced until biomass reached 100 t ha^{-1}. After that point, the increase in woody backscatter was reduced but biomass still increased to around –8 dB at about 500 t ha^{-1} of total AGB.

When applied to independent data, the RMSE of the proposed regression models based on DWT ranged from 117 to 128 t ha^{-1} (35–38%) of mean AGB. The RMSE of the validation data was higher than in the regression models, as shown in Tables 3 and 4; possible explanations are differences in species composition and stand density among sample plots. Those differences may have led to two sample plots with similar levels of AGB to demonstrate different reflectance. In comparison, Lefsky et al. (2005) also found an RMSE of 118.5 t ha^{-1} when estimating AGB using a light detection and ranging image. Saachi et al. (2011) found that the estimation accuracy of AGB was affected by the size of sample plots, the type of wavelength and polarization, and the use of interferometric SAR (InSAR) to measure tree height. At a maximum AGB of 300 t ha^{-1}, the RMSE of the validation using the L-band with full polarization (HH, HV, and VV) was 39.5 and 33.1 t ha^{-1} for sample plots of 0.50 and 1.0 ha, respectively, and for the full polarization integrated with the InSAR

at the same plot size, RMSE was 30.8 and 29.0 t ha^{-1}, respectively (Saachi et al. 2011). For the P-band with the same maximum AGB and 0.5 ha of the sample plot, the obtained RMSEs were 26.6 and 20.2 ton ha^{-1} and for 1.0 ha of sample plot the RMSEs were 19.9 and 15.1 ton ha^{-1} for full polarization and full polarization integrated with InSAR, respectively. For the current study area, further study to reduce the RMSE of estimated AGB could be conducted by increasing the size of sample plot, the use of P-bands, or integration with the InSAR.

5. Conclusions

The proposed model shows the potential use of PALSAR data when integrated with Landsat-7 ETM+ or fraction images. DWT qualitatively and quantitatively improved the performance of the model. Fusion using DWT visually provides similar results to multispectral images. The integration of radar and optical imagery increased the estimation accuracy of AGB in mixed dipterocarp forest. The proposed models fused fraction images with PALSAR data, thereby significantly increasing the coefficient of determination compared with models based only on radar backscatter. The proposed regression models using DWT have a lower RMSE (by 18–25%) compared with the Brovey transform when applied to the independent data set. The current regression models also reduced RMSE (by 10–12%) compared with the model derived only from spectral mixture analysis.

Acknowledgements

We thank B.T. Sasongko, Bogor Agriculture University, for helpful discussions on PALSAR. The authors are grateful to Dr M.J. Canty for the DWT script, W. Nieuwenhuis for technical assistance, and my colleague, Claudia Pittiglio, for an in-depth discussion on wavelet theory. This research was supported by a grant from The Netherlands Fellowship Programme (NFP).

References

Acerbi-Junior, F. W., J. G. P. Clevers, and M. E. Schepmna. 2006. "The Assessment of Multi-Sensor Image Fusion Using Wavelet Transforms for Mapping the Brazilian Savanna." *International Journal of Applied Earth Observation and Geoinformation* 8: 278–288.

Adams, J. B., and A. R. Gillespie. 2006. Remote *Sensing* of *Landscapes* with *Spectral Images: A Physical Modeling Approach*, 126–164. London: Cambridge University Press.

Addison, P. S. 2002. *The Illustrated Wavelet Transform Handbook. Introductory Theory and Applications in Science, Engineering, Medicine and Finance*, 1–91. London: Institute of Physics.

Alaska Satellite Facility Engineering Group. 2009. *ASF Map Ready User Manual*. Accessed November 8, 2009. http://www.asf.alaska.edu/sardatacenter/softwaretools

Alparone, L., S. Baronti, A. Garzelli, and F. Nencini. 2004. "Landsat ETM+ and SAR Image Fusion Based on Generalized Intensity Modulation." *IEEE Transactions on Geoscience and Remote Sensing* 42: 2832–2839.

Amolins, K., Y. Zhang, and P. Dare. 2007. "Wavelet Based Image Fusion Techniques—an Introduction, Review and Comparison." *ISPRS Journal of Photogrammetric and Remote Sensing* 62: 249–263.

Austin, J. M., B. G. Mackey, and K. P. van Nief. 2003. "Estimating Forest Biomass Using Satellite Radar: An Exploratory Study in a Temperate Australian Eucalyptus Forest." *Forest Ecology and Management* 176: 5755–5783.

Balzter, H., L. Skinner, A. Luckman, and R. Brooke. 2003. "Estimation of Tree Growth in a Conifer Plantation over 19 Years from Multi-Satellite L-Band SAR." *Remote Sensing of Environment* 84: 184–191.

Basuki, T. M., P. E. van Laake, A. K. Skidmore, and Y. A. Hussin. 2009. "Allometric Equations for Estimating the Above-Ground Biomass in Tropical Lowland *Dipterocarp* Forests." *Forest Ecology and Management* 257: 1684–1694.

Bertault, J., and K. Kadir, K. 1998. *Silvicultural Research in a Lowland Mixed Dipterocarp Forest of East Kalimantan: The Contribution of STREK Project*. Bogor, Indonesia: CIRAD Forêt, FORDA and P.T. Inhutani I.

Boardman, J. M., F. A. Kruse, and R. O. Green. 1995. "Mapping Target Signature via Partial Unmixing of AVIRIS Data." *Summaries of the Fifth JPL Airborne Earth Science Workshop*. JPL, 95, 23–26.

Bradshaw, G. A., and T. Spies. 1992. "Characterizing Canopy Gap Structure in Forests Using Wavelet Analysis." *Journal of Ecological Society* 80: 205–215.

Bruce, L. M., C. Morgan, and S. Larsen. 2001. "Automated Detection of Subpixel Hyperspectral Targets with Continuous and Discrete Wavelet Transforms." *IEEE Transactions on Geoscience and Remote Sensing* 39: 2217–2226.

Cakir, H. I., S. Khorram, X. L. Dai, and P. de Fraipont. 1999. *Merging SPOT XS Imagery Using the Wavelet Transform Method to Improve Classification Accuracy*. 0-7803-5207-6/99/$10.00©1999 *IEEE*, 71–73.

Canty, M. J. 2010. *Image Analysis, Classification and Change Detection in Remote Sensing with Algorithms for ENVI/IDL*, 73–387. 2nd ed. New York: Taylor & Francis.

Chavez, P. S., S. C. Sides, and J. A. Anderson. 1991. "Comparison of Three Different Methods to Merge Multiresolution and Multispectral Data: Landsat TM and SPOT Panchromatic." *Photogrammetric Engineering & Remote Sensing* 57: 295–303.

Chen, W., D. Blain, J. Li, K. Keohler, R. Fraser, Y. Zhang, S. Leblanc, I. Olthof, J. Wang, and M. Mcgovern. 2009. "Biomass Measurements and Relationships with Landsat-7/ETM+ and JERS-1/SAR Data over Canada's Western Sub-Arctic and Low Arctic." *International Journal of Remote Sensing* 30: 2355–2376.

Chibani, Y. 2005. "Selective Synthetic Aperture Radar and Panchromatic Image Fusion by Using the à Trouswavelet Decomposition." *EURASIP Journal on Applied Signal Processing* 14: 22072–22214.

Chibani, Y. 2006. "Additive Integration of SAR Features into Multispectral SPOT Images by Means of the À Trous Wavelet Decomposition." *ISPRS Journal of Photogrammetric & Remote Sensing* 60: 306–314.

Chibani, Y., and A. Houacine. 2003. "Redundant Versus Orthogonal Wavelet Decomposition for Multisensory Image Fusion." *Pattern Recognition* 36: 879–887.

EXELIS Visual Information Solutions. 2013. ENVI™ Environment for Visualizing Images and IDL™ Interactive Data Language. Accessed March 20, 2013. http://www.exelisvis.com/ProductsServices/ENVI.aspx

Fransson, J. E. S., F. Walter, and L. M. H. Ulander. 2000. "Estimation of Forest Parameters Using CARABAS-II VHF SAR Data." *IEEE Transaction on Geoscience and Remote Sensing* 38: 720–727.

Gemmell, F. M. 1995. "Effects of Forest Cover, Terrain, and Scale on Timber Volume Estimation with Thematic Mapper Data in the Rocky Mountain Site." *Remote Sensing of Environment* 51: 291–305.

Huang, X., L. Zhang, and P. Li. 2008. "A Multiscale Feature Fusion Approach for Classification of Very High Resolution Satellite Imagery Based on Wavelet Transform." *International Journal of Remote Sensing* 29: 5923–5941.

Hussin, Y. A., and S. R. Shaker. 1996. "Optical and Radar Satellite Image Fusion Techniques for Monitoring Natural Resources and Land Use Changes." *The German International Journal of Electronic and Communications*. AEU EUSAR'96 Special Issue, 169–176.

Hyde, P., R. Nelso, D. Kimes, and E. Levine. 2007. "Exploring LiDAR–RaDAR Synergy—Predicting Aboveground Biomass in a Southwestern Ponderosa Pine Forest Using LiDAR, SAR and InSAR." *Remote Sensing of Environment* 106: 28–38.

Kellndorfer, J. M., M. C. Dobson, J. D. Vona, and M. Clutter. 2003. "Toward Precision Forestry: Plot-Level Parameter Retrieval for Slash Pine Plantations with JPL IRSAR." *IEEE Transactions on Geoscience and Remote Sensing* 41: 1571–1582.

Kellndorfer, J. M., L. E. Pierce, and M. C. Dobson. 1998. "Toward Consistent Regional-to-Global-Scale Vegetation Characterization Using Orbital SAR System." *IEEE Transactions on Geoscience and Remote Sensing* 36: 1396–1411.

Kumar, A. S., B. Kartikeyan, and K. L. Majumdar. 2000. "Band Sharpening of IRS-Multispectral Imagery by Cubic Spline Wavelets." *International Journal of Remote Sensing* 21: 581–594.

Kuplich, T. M., P. J. Curran, and P. M. Atkinson. 2005. "Relating SAR Image Texture to the Biomass of Regenerating Tropical Forests." *International Journal of Remote Sensing* 26: 4829–4854.

Lefsky, M. A., D. P. Turner, M. Guzy, and W. B. Cohen. 2005. "Combining Lidar Estimates of Aboveground Biomass and Landsat Estimates of Stand Age for Spatially Extensive Validation of Modeled Forest Productivity." *Remote Sensing of Environment* 95: 549–558.

Leica Geosystem. 2008. *ERDAS Field Guide™*, 335 pp. Atlanta, GA: ERDAS Inc.

Lemeshewsky, G. P. 1999. "Multispectral Multisensor Image Fusion Using Wavelet Transforms." *Proceedings of SPIE International Society for Optical Engineering*, *Visual Image Processing VIII*, Orlando, USA, 3716: 214–222.

Li, S., J. T. Kwok, and Y. Wang. 2002. "Using the Discrete Wavelet Frame Transformation to Merge Landsat TM and SPOT Panchromatic Images." *Information Fusion* 3: 17–23.

Liang, P., M. Moghaddam, L. Pierce, and R. M. Lucas. 2005. "Radar Backscatter Model for Multi-Layer Mixed Species Forests." *IEEE Transactions on Geoscience and Remote Sensing* 43: 2612–2626.

Lu, D. 2006. "The Potential and Challenge of Remote Sensing-Based Biomass Estimation." *International Journal of Remote Sensing* 27: 1297–1328.

Lu, D., M. Batistella, and E. Moran. 2005. "Satellite Estimation of Aboveground Biomass and Impacts of Forest Stand Structure." *Photogrammetric Engineering & Remote Sensing* 71: 967–974.

Lucas, R. M., N. Cronin, A. Lee, M. Moghaddam, C. Witte, and P. Tickle. 2006. "Empirical Relationships Between AIRSAR Backscatter and LiDAR-Derived Forest Biomass, Queensland, Australia." *Remote Sensing of Environment* 100: 407–425.

Lucas, R. M., M. Moghaddam, and N. Cronin. 2004. "Microwave Scattering From Mixed-Species Forests, Queensland, Australia." *IEEE Transactions on Geoscience and Remote Sensing* 42: 2142–2159.

Luckman, A., J. Baker, M. Honzák, and R. Lucas. 1998. "Tropical Forest Biomass Density Estimation Using JERS-1 SAR: Seasonal Variation, Confidence Limits, and Application to Image Mosaic." *Remote Sensing of Environment* 63: 126–139.

Mallat, S. G. 1989. "A Theory for Multiresolution Signal Decomposition: The Wavelet Representation." *IEEE Transactions on Pattern Analysis and Machine Intelligence* 11: 674–693.

Martinez, B., and M. A. Gilabert. 2009. "Vegetation Dynamics from NDVI Time Series Analysis Using the Wavelet Transform." *Remote Sensing of Environment* 113: 1823–1842.

Musa, M. K., Y. A. Hussin, and M. C. Weir. 2004. "Multi-Data Fusion for Sustainable Forest Management." *Asian Journal on Geoinformatics* 4: 57–70.

Núnêz, J., X. Otazu, O. Fors, A. Prades, V. Palà, and R. Arbiol. 1999. "Multiresolution-base Image Fusion with Additive Wavelet Decomposition." *IEEE Transactions on Geoscience and Remote Sensing* 37: 1204–1211.

Pajares, G., and J. M. de la Cruz. 2004. "A Wavelet-Based Image Fusion Tutorial." *Pattern Recognition* 37: 1855–1872.

Phat, N. K., W. Knorr, and S. Kim. 2004. "Appropriate Measures for Conservation of Terrestrial Carbon Stocks—Analysis of Trends of Forest Management in Southeast Asia." *Forest Ecology and Management* 191: 283–299.

Pittiglio, C., A. K. Skidmore, C. A. J. M. de Bie, and A. Murwira. 2012. "A Common Dominant Scale Emerges from Images of Diverse Satellite Platforms Using the Wavelet Transform." *International Journal of Remote Sensing* 32: 3665–3687.

Pohl, C., and J. L. van Genderen. 1998. "Multisensor Image Fusion in Remote Sensing: Concepts, Methods, and Applications." *International Journal of Remote Sensing* 19: 823–854.

Pradhan, P. S., R. L. King, N. H. Youman, and D. W. Holcom. 2006. "Estimation of the Number of Decomposition Levels for a Wavelet-Based Multiresolution Multisensor Image Fusion." *IEEE Transactions on Geoscience and Remote Sensing* 44: 3674–3686.

Pu, R., and P. Gong. 2004. "Wavelet Transform Applied to EO-1 Hyperspectral Data for Forest LAI and Crown Closure Mapping." *Remote Sensing of Environment* 91: 212–224.

Ranchin, T., and L. Wald. 2000. "Fusion of High Spatial and Spectral Resolution Images: The ARSIS Concept and Its Implementation." *Photogrammetric Engineering and Remote Sensing* 66: 49–61.

Rauste, Y. 2005. "Multi-Temporal JERS SAR Data in Boreal Forest Biomass Mapping." *Remote Sensing of Environment* 97: 263–725.

Ronsenqvist, A., A. Milne, R. Lucas, M. Imhoff, and C. Dobson. 2003. "A Review of Remote Sensing Technology in Support of the Kyoto Protocol." *Environmental Science & Policy* 6: 441–445.

Saatchi, S., M. Marlier, R. L. Chazdon, D. B. Clark, and A. E. Russell. 2011. "Impact of Spatial Variability of Tropical Forest Structure on Radar Estimation of Aboveground Biomass." *Remote Sensing of Environment* 115: 2836–2849.

Santos, J. R., C. C. Freitas, L. S. Araujo, L. V. Dutra, J. C. Mura, F. F. Gama, L. S. Soler, and S. J. S. Sant'Anna. 2003. "Airborne P-Band SAR Applied to the Aboveground Biomass Studies in the Brazilian Tropical Rainforest." *Forest Ecology and Management* 87: 482–493.

Schimel, D. S., J. I. House, K. A. Hibbard, P. Bousquet, P. Ciais, P. Peylin, B. H. Braswell, M. J. Apps, D. Baker, A. Bondeau, J. Canadell, G. Churkina, W. Cramer, A. S. Denning, C. B. Field, P. Friedlingstein, C. Goodale, M. Heimann, R. A. Houghton, J. M. Melillo, B. Moore, III, D. Murdiyarso, I. Noble, S. W. Pacala, I. C. Prentice, M. R. Raupach, P. J. Rayner, R. J. Scholes, W. L. Steffen, and C. Wirth. 2001. "Recent Patterns and Mechanisms of Carbon Exchange by Terrestrial Ecosystems." *Nature* 414: 169–172.

Shensa, M. J. 1992. "The Discrete Wavelet Transform: Wedding the Â Trous and Mallat Algorithms." *IEEE Transactions and Signal Processing* 40: 2464–2482.

Shi, W., C. Zhu, C. Zhu, and X. Yang. 2003. "Multi-Band Wavelet for Fusing SPOT Panchromatic and Multiband Images." *Photogrammetric Engineering & Remote Sensing* 69: 513–520.

Simone, G., A. Farina, F. C. Morabito, S. B. Serpico, and L. Bruzzone. 2002. "Image Fusion Techniques for Remote Sensing Applications." *Information Fusion* 3: 3–15.

Sist, P., and A. Saridan. 1998. "Description of the Primary Lowland Forest of Berau." In *Sylvicultural Research in a Lowland Mixed Dipterocarp Forest of East Kalimantan*, edited by J. Bertault and K. Kadir, 51–73. Montpellier: Cirad-Forêt.

Souza, C. M. Jr., D. A. Roberts, and M. A. Cocrane. 2005. "Combining Spectral and Spatial Information to Map Canopy Damage from Selective Logging and Forest Fires." *Remote Sensing of Environment* 98: 329–343.

Steininger, M. K. 2000. "Satellite Estimation of Tropical Secondary Forest Above-Ground Biomass Data from Brazil and Bolivia." *International Journal of Remote Sensing* 21: 1139–1157.

Strand, E. K., A. M. S. Smith, S. C. Bunting, L. A. Vierling, D. B. Hann, and P. E. Gessler. 2006. "Wavelet Estimation of Plant Spatial Patterns in Multitemporal Aerial Photography." *International Journal of Remote Sensing* 27: 2049–2054.

Strang, G., and T. Nguyen. 1997. *Wavelets and Filter Banks*, 103–52. New York: Wellesley-Cambridge Press.

Tompkins, S., J. F. Mustard, C. M. Pieters, and D. W. Forsyth. 1997. "Optimization of Endmembers for Spectral Mixture Analysis." *Remote Sensing of Environment* 59: 472–489.

Trevett, J. W. 1986. "Imaging Radar for Resources Surveys." In *Remote Sensing Application*, edited by E. C. Barret and L. F. Curtis, 17–62. New York: Chapman and Hall.

Tsolmon, R., R. Tateishi, and J. S. S. Tetuko. 2002. "A Method to Estimate Forest Biomass and its Application to Monitor Mongolian Taiga Using JERS-1 SAR Data." *International Journal of Remote Sensing* 23: 4971–4978.

Vega, B. 2005. "Image Fusion of Optical and Microwave Data to Assess Criteria and Indicator (C&I) Related to Forest Encroachment, for Certification Process of Sustainable Forest Management (SFM)." 79 pp. Unpublished MSc thesis, ITC, Enschede.

Wang, C., and J. Qi. 2008. "Biophysical Estimation in Tropical Forests Using JERS-1 SAR and VNIR Imagery II. Above-Ground Woody Biomass." *International Journal of Remote Sensing* 29: 6827–6849.

Wang, Z., D. Ziou, C. Armenakis, L. Deren, and Q. Li. 2005. *IEEE Transactions on Geoscience and Remote Sensing* 43: 1391–1402.

Yunhao, C., D. Lei, L. Jing, L. Xiaobing, and S. Peijun. 2006. "A New Wavelet-Based Image Fusion Method for Remotely Sensed Data." *International Journal of Remote Sensing* 27: 1465–1476.